Supersymmetric Transformations in Optical Fibers

Andrés Macho, Roberto Llorente, and Carlos García-Meca

Supersymmetric Transformations in Optical Fibers

Andrés Macho,[*] Roberto Llorente and Carlos García-Meca,[*]

Nanophotonics Technology Center, Universitat Politècnica de València, 46022 Valencia, Spain
e-mail address: amachor@ntc.upv.es, cargarm2@ntc.upv.es

Supersymmetry (SUSY) has recently emerged as a tool to design unique optical structures with degenerate spectra. Here, we study several fundamental yet so far unexplored aspects and variants of one-dimensional SUSY in axially-symmetric optical media, including their basic spectral features and the conditions for degeneracy breaking. Surprisingly, we find that the SUSY degeneracy theorem is partially (totally) violated in optical systems connected by isospectral (broken) SUSY transformations due to a degradation of the paraxial approximation. In addition, we show that isospectral constructions provide a dimension-independent design control over the group delay in SUSY fibers. Moreover, we find that the studied unbroken and isospectral SUSY transformations allow us to generate refractive index superpartners with an extremely large phase-matching bandwidth, spanning the S+C+L optical bands. These singular features define a new class of optical fibers with unprecedented potential applications. To illustrate this, we numerically demonstrate the possibility of building photonic lanterns supporting broadband heterogeneous supermodes with large effective area, a broadband all-fiber true mode (de)multiplexer requiring no mode conversion, and different mode filtering, mode conversion and pulse shaping devices. Finally, we discuss the possibility of extrapolating our results to acoustics and quantum mechanics.

I. INTRODUCTION

Supersymmetry was originally introduced within the context of string and quantum field theory as a necessary ingredient to unify the basic interactions of nature, i.e. strong, electroweak, and gravitational interactions [1]−[8]. For particle theorists, SUSY also offers a mathematical framework upon which to propose different dark matter particle candidates [9]−[12]. Despite these interesting features of supersymmetric models, there has been no experimental evidence of SUSY in nature so far [13]. Nevertheless, the ideas of SUSY have been profitably extended to diverse areas of physics and engineering [14]−[29], with applications to, e.g., quantum cascade lasers [20], graphene field theory [21], or matter-wave circuits [22].

One-dimensional (1D) SUSY has attracted particular attention in the fields of nonrelativistic quantum mechanics and photonics [14],[23]−[29]. The superalgebra underneath 1D SUSY transformations (also known as Darboux or Darboux-Crum transformations) allows us to relate two different real quantum or optical potentials with identical spectra and scattering properties in the Helmholtz regime [14],[24]. These supersymmetric potentials are usually termed as superpartners. Moreover, efforts have been undertaken to extend the degeneracy and the scattering relations of 1D SUSY to complex potentials exhibiting parity-time symmetry [16]−[19],[29]. In such a scenario, it has been observed that superpartners exhibit dissimilar reflection coefficients [29].

Thanks to these interesting features, new real and complex quantum potentials have been found to be analytically solvable [14]−[19], and a novel class of supersymmetric 1D optical devices has been recently proposed with intriguing and unexpected properties for mode multiplexing, mode conversion and cloaking applications [24]−[29].

Remarkably, the ideas of 1D SUSY can also be applied to *n*-dimensional potentials [14],[30]. As an example, one can reduce the 3D Schrödinger equation to a 1D equation in spherical systems with radial symmetry [30], enabling us to benefit from the unique features of 1D SUSY. In the same way, one could expect the advantages of 1D SUSY to be also exploitable in axially-symmetric systems.

Physical systems with axial symmetry present particular interest not only in quantum mechanics [31],[32], but also in other branches of physics, such as acoustics and photonics. In acoustics, cylindrical ducts are of special interest for pressure wave propagation and turbocharger applications [33]−[36]. In photonics, axially-symmetric media can be found in single- and multi-core optical fibers, optical couplers, laser arrays, modulators and Bragg gratings [37]−[41].

Along this line, Miri et al. reported a theoretical SUSY relation between the azimuthal Bessel modes of two optical fibers [24] and its potential application to angular momentum multiplexing [42]. However, the study was limited to the unbroken SUSY regime, while many aspects of SUSY theory still remain unexplored in this context. Firstly, the different spectral features of SUSY axially-symmetric optical systems (such as bandwidth and group delay) has not been studied so far. Secondly, the SUSY formalism encompasses a rich toolbox, including, e.g., unbroken SUSY chains, broken SUSY transformations, and isospectral deformations (having the same energy levels as
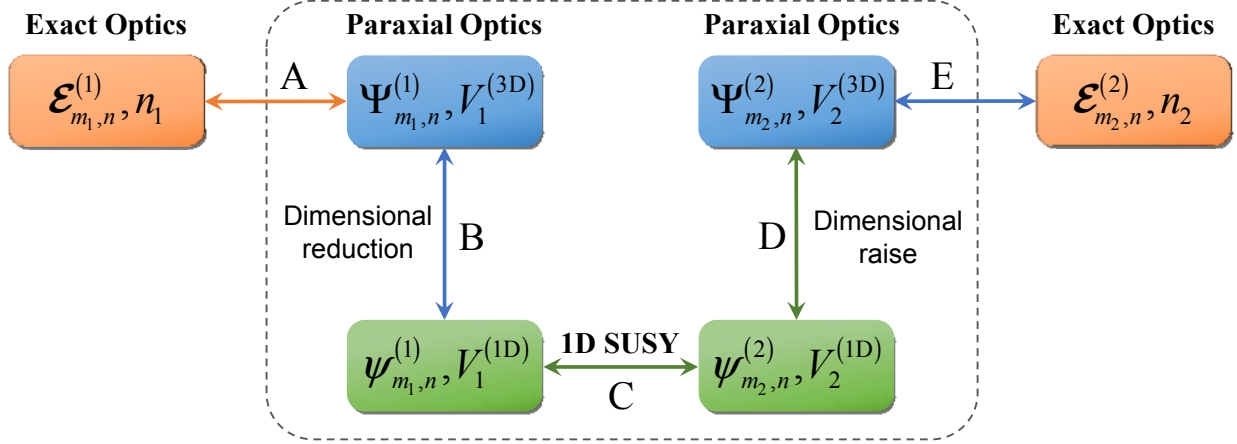
FIG. 1. Flowchart of transformations to apply 1D SUSY to 3D axially-symmetric optical potentials.

the original system), which have not been analyzed within the frame of axially-symmetric media. Thirdly, the application of SUSY to this kind of systems entails a series of steps and assumptions whose range of validity has not yet been assessed: the dimensional reduction of the Helmholtz equation from 3D to 1D, the subsequent appearance of singularities in the superpotential relating the superpartners, and the accuracy of the required slowly-varying index (SVI) and paraxial approximations in the photonic case.

For instance, a singular superpotential can give rise to a breakdown of the degeneracy theorem between superpartners [14],[43]−[46], and therefore, its impact on the corresponding mode multiplexing applications should be critically investigated. Moreover, as we will show, the paraxial approximation is no longer valid (except for some energy levels) in broken SUSY and isospectral constructions, leading to unexpected effects and novel functionalities.

In this work, we study all these points within the context of photonics. As a byproduct, a variety of applications for mode filtering, mode conversion, mode multiplexing, supermode generation (linear combination of degenerate modes of close-packed waveguides), dispersion engineering and pulse shaping are proposed. Specifically, using unbroken SUSY transformations, we design a multi-core fiber (MCF) incorporating mode conversion, mode filtering, and pulse shaping functionalities in the S+C+L optical bands (1460-1625 nm), as well as a photonic lantern supporting broadband heterogeneous supermodes generated from the linear combination of degenerate fiber modes with different azimuthal and radial order. In addition, we show that the partial degeneracy associated with isospectral photonic SUSY fibers can be used to build a broadband all-fiber true mode (de)multiplexer requiring no mode conversion, and that this approach offers a dimension-independent design control over the group delay of the fiber modes. To verify and illustrate these utilities, extensive

numerical simulations are performed using a 3D electromagnetic mode solver (CST Microwave Studio and COMSOL Multiphysics).

The paper is structured as follows. In Section II, we describe the transformation method proposed to apply 1D SUSY to 3D axially-symmetric optical potentials. In Section III, we explore unbroken and broken 1D SUSY transformations of these systems. The construction of isospectral potentials via the Darboux procedure is investigated in Section IV. Finally, in Section V, the main conclusions and applications of this work are highlighted, including the extension of the presented theory to acoustics and quantum mechanics.

II. 1D SUSY IN AXIALLY-SYMMETRIC OPTICAL POTENTIALS

We are interested in the bound modes (corresponding to a discrete spectrum of energy levels) of an axially-symmetric linear isotropic non-magnetic optical medium with a refractive index $n(r)$ (with variations confined to a finite spatial region). Such a system is described by the following exact 3D wave equation (cylindrical coordinates r, φ, z):

$$\nabla \times \nabla \times \mathcal{E}_{m,n}(\mathbf{r}, \omega) - \frac{\omega^2}{c_0^2} n^2(r) \mathcal{E}_{m,n}(\mathbf{r}, \omega) = \mathbf{0}, \qquad (1)$$

where ω is the angular frequency, c_0 is the speed of light at the vacuum, and $\mathcal{E}_{m,n}(\mathbf{r},\omega)$ is the Fourier transform of the electric field strength of the eigenmode mn, with m and n indicating respectively the azimuthal and radial order. Note that Eq. (1) allows us to work with dispersive media just by using the proper frequency-dependent expression for $n(r)$, although we only considered non-dispersive media to facilitate the analysis.

In particular, we focus on the possibility of applying 1D SUSY to Eq. (1) through the scheme shown in Fig. 1. We start from a given system $[\mathcal{E}_{m1,n}^{(1)}, n_1]$ satisfying Eq. (1).

For SVI media, that is, with $\delta n \ll n$ in $\delta r \sim n\lambda_0$ (where $\delta n := |n(r) - n(r+\delta r)|$ and $\lambda_0 = 2\pi c_0/\omega$ is the free-space wavelength) and under the paraxial approximation (for which the longitudinal component of $\mathcal{E}_{m,n}$ can be neglected [37]), Eq. (1) reduces to (step A):

$$\left[\Delta + E_{m,n}^{(3D)} - V^{(3D)}(r)\right]\Psi_{m,n}(\mathbf{r}) = 0, \qquad (2)$$

where Δ is the Laplacian operator, $E_{m,n}^{(3D)} - V^{(3D)}(r) \equiv (\omega^2/c_0^2)n(r)$, and $\Psi_{m,n}$ is the linear combination of the transversal component of the quasi-degenerate true modes. This corresponds, for instance, to the linearly-polarized $LP_{m,n}$ mode group of a weakly-guiding optical fiber [37]. Since there is a degree of freedom in the mathematical identification of $E_{m,n}^{(3D)} - V^{(3D)}(r)$ with the refractive index, we take $E_{m,n}^{(3D)} \equiv 0$ for simplicity (it will be nonzero in quantum systems, see Table I in Section V). Therefore, it is important to bear in mind that $E_{m,n}^{(3D)}$ is just an auxiliary mathematical quantity different from the physical field energy. In Section 1 of the supplemental material, we include a more detailed discussion of Eq. (2).

At this point, we perform a dimensional reduction from the 3D system $[\Psi_{m1,n}^{(1)}, V_1^{(3D)}]$ to the 1D system $[\psi_{m1,n}^{(1)}, V_1^{(1D)}]$ (step B, see below). Then, we transform $[\psi_{m1,n}^{(1)}, V_1^{(1D)}]$ into $[\psi_{m2,n}^{(2)}, V_2^{(1D)}]$ using 1D SUSY (step C). Proceeding in a similar manner as in the previous dimensional reduction, we calculate the 3D system $[\Psi_{m2,n}^{(2)}, V_2^{(3D)}]$ from $[\psi_{m2,n}^{(2)}, V_2^{(1D)}]$ (step D). Finally, $\Psi_{m2,n}^{(2)}$ can be identified with the transversal component of the true modes of a second optical system $[\mathcal{E}_{m2,n}^{(2)}, n_2]$ (step E) SUSY-connected with $[\mathcal{E}_{m1,n}^{(1)}, n_1]$, provided that the SVI and paraxial approximations apply to n_2.

The dimensional reduction of Eq. (2) can be performed by applying the following separation of variables to $\Psi_{m,n}$:

$$\Psi_{m,n}(\mathbf{r}) = R_{m,n}(r)e^{im\varphi}e^{-i\beta_{m,n}z}, \qquad (3)$$

with $R_{m,n}$ the function describing the radial dependence and $\beta_{m,n}$ the phase constant of the eigenmode. Now, using the transformation $R_{m,n}(r) = r^{-1/2}\psi_{m,n}(r)$, Eq. (2) is reduced to:

$$\left[\frac{d^2}{dr^2} + E_{m,n}^{(3D)} - \left(\beta_{m,n}\right)^2 - V^{(3D)}(r) - \frac{m^2}{r^2} + \frac{1}{4r^2}\right]\psi_{m,n}(r) = 0. \quad (4)$$

Eq. (4) matches the following 1D Helmholtz equation:

$$\left[\frac{d^2}{dr^2} + E_n^{(1D)} - V^{(1D)}(r)\right]\psi_{m,n}(r) = 0, \qquad (5)$$

with the identification:

$$E_n^{(1D)} - V^{(1D)}(r) = E_{m,n}^{(3D)} - \left(\beta_{m,n}\right)^2 - V^{(3D)}(r) - \frac{m^2}{r^2} + \frac{1}{4r^2}. \quad (6)$$

In order to obtain a well-defined eigenvalue problem, an adequate expression for $E_n^{(1D)}$ and $V^{(1D)}(r)$ must be selected. Obviously, the spatially-dependent terms of the right-hand

side of Eq. (6) should be identified with $V^{(1D)}(r)$ (assuming a constant value of m). With this consideration in mind, a possible choice is (other options are accounted for by introducing a free-parameter α, see below):

$$E_n^{(1D)} = E_{m,n}^{(3D)} - \left(\beta_{m,n}\right)^2; \qquad (7)$$

$$V^{(1D)}(r) = V^{(3D)}(r) + \frac{m^2}{r^2} - \frac{1}{4r^2}. \qquad (8)$$

Crucially, the various steps and approximations of the described method may alter the ideal SUSY relation between $\mathcal{E}_{m1,n}^{(1)}$ and $\mathcal{E}_{m2,n}^{(2)}$. This possibility has not been analyzed so far and will be essential for some of the most interesting results derived from our study (especially in isospectral constructions). In particular, the following considerations are in order:

- From Eq. (8), inverse-square potentials $V^{(1D)}(r)$ appear for a non-singular $V^{(3D)}(r)$ (as will be our case). The corresponding 1D eigenvalue problem [Eq. (5)] may be ill-defined if it is not possible to choose a unique basis of eigenfunctions based on square integrability and boundary conditions [47]. Fortunately, this is never the case for $m \geq 0$ [48], guarantying the validity of the mapping between Eqs. (2) and (5) established by Eqs. (3) and (8) in step B.

- As we will see later, inverse-square potentials relate to a singular superpotential in the SUSY transformations. As a consequence, the degeneracy between $V_1^{(1D)}$ and $V_2^{(1D)}$ will only be preserved if the SUSY bound states $\psi_{m2,n}^{(2)}$ are continuous normalizable solutions [14].

- The transformation $R_{m,n}(r) = r^{-1/2}\psi_{m,n}(r)$ may give rise to a breakdown of the degeneracy between $V_1^{(3D)}$ and $V_2^{(3D)}$ if the optical boundary conditions are violated, that is, if $R_{m2,n}^{(2)}$ becomes singular at $r = 0$ after step D.

- The complete degeneracy between $V_1^{(3D)}$ and $V_2^{(3D)}$ may also be broken if n_1 or n_2 do not approximately satisfy the SVI criterion or their true modes do not meet the paraxial approximation.

We will check all these points in the considered SUSY transformations. To simplify the discussion, we will use the more economical notation $V^{(1D)}(r) \equiv V(r)$ and $E_n^{(1D)} \equiv E_n$ ($n = 1,2,3\ldots$) from now on.

III. UNBROKEN AND BROKEN 1D SUSY

For a given potential $V_1(r)$ with energy levels $E_n^{(1)}$, SUSY provides a systematic way for generating a potential $V_2(r)$ with energy levels $E_n^{(2)}$ equal to those of $V_1(r)$, with the possible exception of the ground state level $E_1^{(1)}$. In the SUSY literature, V_2 is usually referred to as the superpartner of V_1. In particular, SUSY is known to be unbroken if the SUSY operator $\hat{A}^-$ (see below) annihilate the ground state wave function of V_1, i.e., $\hat{A}^-\psi_{m1,1}^{(1)} = 0$, which corresponds with the case $E_1^{(1)} = 0$ [6],[14]. In this scenario, V_2 has the same energy levels as V_1 except for

$E_1^{(1)}$, i.e., $E_n^{(2)} = E_{n+1}^{(1)}$. On the contrary, SUSY is spontaneously broken when $\hat{A}^- \psi_{m1,1}^{(1)}$ generates a non-vanishing normalizable solution of V_2, in which case $E_1^{(1)} \neq 0$ and both spectra are found to be completely degenerate (except perhaps for singular superpotentials), that is, $E_n^{(2)} = E_n^{(1)}$ [14]. In general, the constraints on SUSY breaking have a far richer scope in quantum field theory than the implications previously described [6]. However, the aforementioned features of SUSY breaking seem to be sufficient for our purposes.

In our case, $E_1^{(1)} = -(\beta_{m1,1})^2 \neq 0$. Therefore, instead of directly calculating a SUSY partner of V_1, it is useful to start from a potential $\hat{V}_1 = V_1 - \alpha$ (associated with the energy-shifted Hamiltonian $\hat{H}_1 = H_1 - \alpha = -d^2/dr^2 + V_1 - \alpha$), calculate its superpartner $\hat{V}_2$ (with a corresponding Hamiltonian $\hat{H}_2 = H_2 - \alpha = -d^2/dr^2 + V_2 - \alpha$), and undo the energy shift to find the superpartner of V_2 as $V_2 = \hat{V}_2 + \alpha$. This allows us to choose between unbroken SUSY or different broken SUSY transformations by selecting $\alpha = E_1^{(1)}$ or $\alpha \neq E_1^{(1)}$, respectively. Assuming V_1 and V_2 of the form:

$$V_i(r) = -\frac{\omega^2}{c_0^2} n_i^2(r) + \frac{m_i^2}{r^2} - \frac{1}{4r^2}; \quad i = 1, 2, \qquad (9)$$

both superpartners are related by the Riccati equation [14]:

$$V_{1,2}(r) = W^2(r) \mp W'(r) + \alpha. \qquad (10)$$

where W is the superpotential. The underlying connection given by Eq. (10) is derived from the properties of the SUSY algebra. More specifically, defining the SUSY Hamiltonian:

$$H = \begin{bmatrix} \hat{H}_1 & 0 \\ 0 & \hat{H}_2 \end{bmatrix}, \qquad (11)$$

and the supercharges:

$$Q^- = \begin{bmatrix} 0 & 0 \\ \hat{A}^- & 0 \end{bmatrix}; \quad Q^+ = \begin{bmatrix} 0 & \hat{A}^+ \\ 0 & 0 \end{bmatrix}, \qquad (12)$$

with $\hat{A}^\pm := \mp d/dr + W(r)$ and $\hat{A}^+ = (\hat{A}^-)^\dagger$ in the case of a real superpotential (where $\dagger$ denotes the Hermitian adjoint operator), the following commutation and anticommutation relations define the closed superalgebra $sl(1/1)$ [14],[15]:

$$[H, Q^\pm] = 0; \quad \{Q^\pm, Q^\mp\} = H; \quad \{Q^\pm, Q^\pm\} = 0. \quad (13)$$

The degeneracy of the spectra is a direct consequence of the fact that Q^+ and Q^- commute with H when a non-singular superpotential is involved [14].

A. Unbroken SUSY

As mentioned before, the unbroken SUSY transformation allows us to connect the spectra of V_1 and V_2 through a relation of the form $E_n^{(2)} = E_{n+1}^{(1)}$. In addition, since $\hat{A}^- \psi_{m1,1}^{(1)} = 0$ and the energy levels are related to the phase constant of the LP modes as indicated by Eq. (7), we will be able to annihilate the ground state $LP_{m1,1}$ and establish a perfect phase-matching between the $LP_{m2,n}^{(2)}$ and $LP_{m1,n+1}^{(1)}$ modes at λ_0. In this vein, outstanding optical applications such as the mode filtering of the $LP_{m1,1}$ mode, mode conversion between a great number of LP modes of different azimuthal (if $m_1 \neq m_2$) and radial order, and supermode generation, can be investigated using the unbroken SUSY procedure. In this context, pulse shaping applications can also be proposed by exploiting the spectral behaviour of V_1 and V_2 at different wavelengths. Finally, some previous works on 1D SUSY suggest that all these interesting features might have a broadband nature, which is an additional motivation to carry out the present study [27]. Before exploring these possibilities, let us first describe the unbroken SUSY transformation in more detail.

A well-known solution of Eq. (10) with $\alpha = E_1^{(1)}$ can be expressed in terms of the ground state wave function $\psi_{m1,1}^{(1)}$ of H_1 as $W(r) = -(\ln \psi_{m1,1}^{(1)}(r))'$ [14]. From the relation $\psi_{m1,1}^{(1)}(r) = r^{1/2} R_{m1,1}^{(1)}(r)$:

$$W(r) = -\frac{d}{dr} \ln \psi_{m_1,1}^{(1)}(r) = -\frac{\left(R_{m_1,1}^{(1)}\right)'}{R_{m_1,1}^{(1)}} - \frac{1}{2r}. \qquad (14)$$

In spite of the fact that Q^+ and Q^- commute with H at $r = 0$ [49], the singularity of W at this point might break the degeneracy between the 1D potentials V_1 and V_2 [43]−[46]. We analytically studied this possibility, finding that any bound state of the form $\psi_{m2,n}^{(2)} \propto \hat{A}^- \psi_{m1,n+1}^{(1)}$ is a continuous normalizable solution, implying that degeneracy between V_1 and V_2 is preserved in all cases [49]. This is consistent with the numerical results obtained via the mode solver of CST Microwave Studio (see below). That is, step C always yields unbroken SUSY-related 1D systems.

On the other hand, an expression for $n_2(r)$ can be derived by combining Eqs. (9), (10) and (14):

$$n_2(r) = \sqrt{n_1^2(r) + 2\frac{c_0^2}{\omega^2}\frac{d^2}{dr^2}\ln\left(r^{\frac{m_1^2 - m_2^2 + 1}{2}} R_{m_1,1}^{(1)}(r)\right)}. \qquad (15)$$

From the above equation, the considered SUSY procedure may also introduce a singularity in $n_2(r)$ at $r = 0$. Although singular potentials have been extensively discussed in the quantum-mechanical literature with interesting physical implications and properties [14],[43],[47], singular refractive indexes pose physical and technological complications in photonics. To avoid this potential hindrance, we search for non-singular refractive indexes by selecting an appropriate value of m_1 and m_2. From the equivalence:

$$R_{m_1,1}^{(1)}(r) \propto J_{m_1}(r) \underset{r \to 0}{\sim} (r/2)^{m_1} / \Gamma(m_1 + 1); \quad m_1 \geq 0, \qquad (16)$$

where J_{m1} is the Bessel function of the first kind and order m_1, and Γ is the Gamma function, we can deduce that the singularity at $r = 0$ is avoided if and only if $n_1(r)$ is non-singular and $m_2 = m_1+1$, with $m_1 \geq 0$. This was already pointed out in [24], although only the case $m_1 = 1$ was analyzed. However, LP modes without azimuthal variation ($m_1 = 0$) are of paramount importance in optical communications, so we will pay particular attention to them in this work.

In addition, it should be noted that Eq. (15) is frequency dependent, not only as a result of the possible frequency changes of n_1, but also of the c_0/ω term and the frequency dependence of $R_{m1,1}^{(1)}$. Consequently, the mentioned phase-matching of SUSY axially-symmetric potentials will be band limited, a fundamental feature that has not been pointed out so far and the implications of which will be carefully studied in this work. Finally, a third parameter that has not yet been analyzed within the frame of optical SUSY is the group delay, i.e., the first-order derivative of the phase constant as a function of the angular frequency.

As an illustrative example that allows us to study all these features (modes without azimuthal variation, band-limited phase-matching, and group delay), we consider an optical fiber (core radius $R_0 = 25$ μm) with a step-index profile n_1 [$n_1 (r \leq R_0) = n_{co}$, $n_1 (r > R_0) = n_{cl}$, see Fig. 2(a)], as the original system. For this configuration, the SVI and paraxial approximations are very accurate, ensuring that, after step A, $\Psi_{m1,n}^{(1)}$ is related to $\mathcal{E}_{m1,n}^{(1)}$ as described above. The same initial index profile will be considered in all the examples analyzed in this paper.

Figure 2(a) shows the profiles of n_2 and W for two different free-space wavelengths ($\lambda_0 = 2\pi c_0/\omega$): 1550 nm and 3000 nm. As expected, n_2 and W are wavelength-dependent, and so will be the phase-matching predicted by Eq. (17).

In the classical modal analysis of step- and gradual-index optical fibers, the spectral features are analyzed from the dispersion and group delay diagrams, which respectively depict the phase constant and the group delay of the LP modes as a function of the angular frequency. In weakly-guiding optical fibers, the above parameters are usually normalized by using the step-index profile as a reference [50]. The normalized phase constant b, normalized frequency v and normalized group delay τ are defined as $b = (\beta/k-n_{cl})/(n_{co}-n_{cl})$, $v = k \cdot R_0 \cdot (n_{co}^2-n_{cl}^2)^{1/2}$ and $\tau = b+v \cdot db/dv$, with $k = \omega/c_0$. In this way, the spectral features of the unbroken SUSY procedure can be analyzed by calculating numerically (via CST Microwave Studio) the aforementioned diagrams for the index profiles $n_1(r)$ and $n_2(r)$.

Figures 2(b)-(d) depict the normalized dispersion and normalized group delay diagrams of the $LP_{m1,n}^{(1)}$ and $LP_{m2,n}^{(2)}$ modes for the cases $m_1 = 0$, 2, $m_2 = m_1+1$ and n varying from 1 to 4 ($\lambda_0 = 1550$ nm). The cases $m_1 = 1$ and $m_1 = 3$ are also included in the supplemental material for
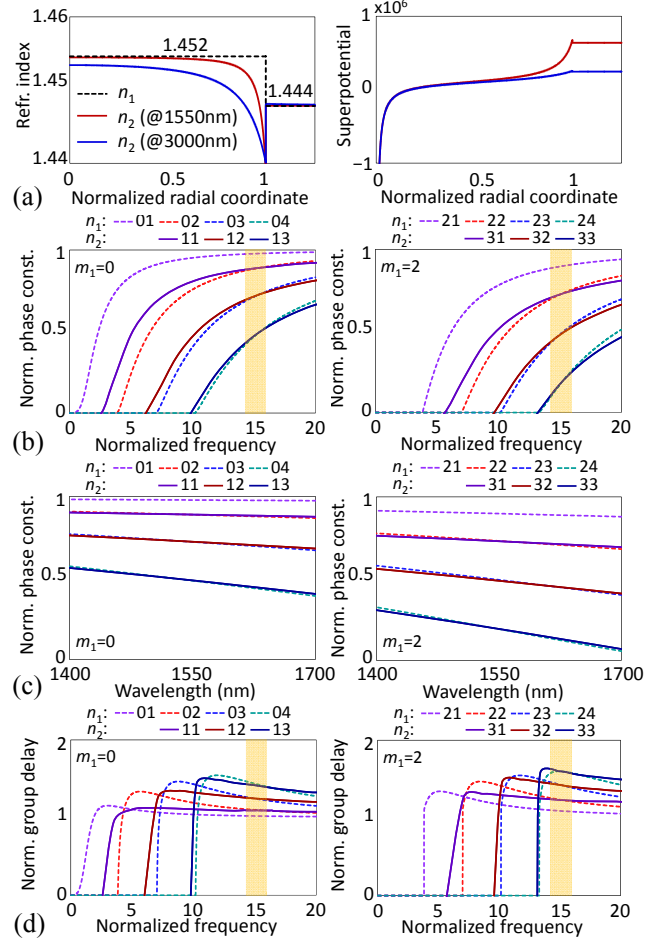
FIG. 2. Modal analysis of two supersymmetric refractive indexes. (a) SUSY partner for the step-index profile and the corresponding superpotential as a function of the normalized radial coordinate (r/R_0). (b) Normalized dispersion diagram of the LP modes as a function of the normalized frequency, and (c) the wavelength comprising the S+C+L optical bands. (d) Normalized group delay as a function of the normalized frequency.

completeness [49]. As seen, in spite of using a singular superpotential, degeneracy between the expected LP modes of both optical systems is present in this case. This inherently implies that step D does not generate unphysical functions $R_{m2,n}^{(2)}$ and that the SVI and paraxial approximations are valid for n_2. Therefore, the unbroken SUSY procedure establishes a perfect phase-matching at λ_0 between the $LP_{m1+1,n}^{(2)}$ and $LP_{m1,n+1}^{(1)}$ eigenmodes, with $m_1 \geq 0$ and $n \geq 1$. More specifically, the corresponding $R_{m,n}(r)$ and $\beta_{m,n}$ are connected by the expressions:

$$\beta_{m_1+1,n}^{(2)} = \beta_{m_1,n+1}^{(1)}; \tag{17}$$

$$R_{m_1+1,n}^{(2)} = \frac{\xi}{\sqrt{r}} \hat{A}^- \left(\sqrt{r} R_{m_1,n+1}^{(1)} \right). \tag{18}$$
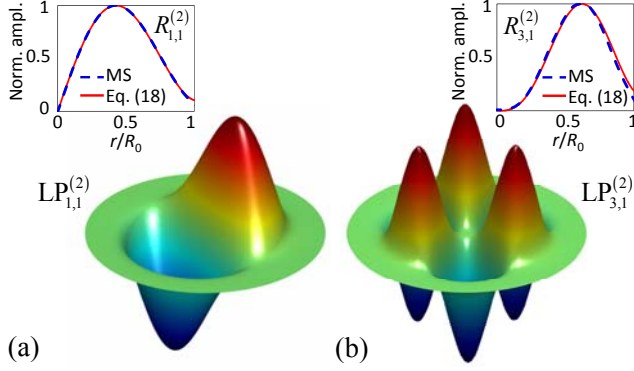
FIG. 3. Ground state wave function $\psi_{m2,1}^{(2)}$ of the SUSY refractive index n_2 for the cases: (a) $m_1 = 0$ and (b) $m_1 = 2$. The comparison between the numerical calculation using the 3D mode solver (MS) and Eq. (18) is inset in the top of the figure.

where ξ is a real constant. In order to validate the previous expression in the analyzed example, we compare in Fig. 3 the results for $R_{m2,1}^{(2)}$ of n_2 for the cases $m_1 = 0$ and $m_1 = 2$ as calculated using Eq. (18) and the 3D mode solver of CST Microwave Studio, finding that both results are in excellent agreement. Notably, an almost perfect phase-matching ($\delta b \leq 0.02$) is achieved between LP modes in an optical bandwidth higher than 300 nm for $m_1 = 0, 2$ [see Fig. 2(c)] and $m_1 = 1,3$ [49]. The above bandwidth is defined as the phase-matching bandwidth (PMBW), which gives information about the range of optical frequencies for which the LP modes of both superpartners are found to be approximately degenerate according to the aforementioned criterion. In real optical fibers, in which the frequency dependence of n_1 and n_2 should also be taken into account, the PMBW could be slightly reduced with respect to the ideal case shown in Fig. 2.

Furthermore, Fig. 2(d) reveals a very interesting feature: the normalized group delay of the LP modes in n_2 presents a weaker frequency dependence than in n_1, which indicates that the supersymmetric optical fiber is less dispersive than the original one. Consequently, the differential mode group delay (DMGD) between the LP modes of n_2 (calculated as the absolute value of the difference between the group delays) is approximately constant within the PMBW.

We next construct an unbroken SUSY chain comprising N supersymmetric refractive indexes $n_1(r),\ldots,n_N(r)$. A given index $n_q(r)$ [$q \in \{2,\ldots,N\}$] can be calculated from the original profile $n_1(r)$ as [49]:

$$n_q(r) = \sqrt{n_1^2(r) + 2\frac{c_0^2}{\omega^2}\frac{d^2}{dr^2}\ln\left(r^{\frac{m_1^2 - m_q^2 + q - 1}{2}}\prod_{i=1}^{q-1} R_{m_i,1}^{(i)}(r)\right)}, \quad (19)$$

with $m_i = m_1 + i - 1$ ($i = 1,\ldots,q$). The phase constants and the wave functions of the q-th system satisfy:

$$\beta_{m_1+q-1,n}^{(q)} = \beta_{m_1,n+q-1}^{(1)}; \quad (20)$$
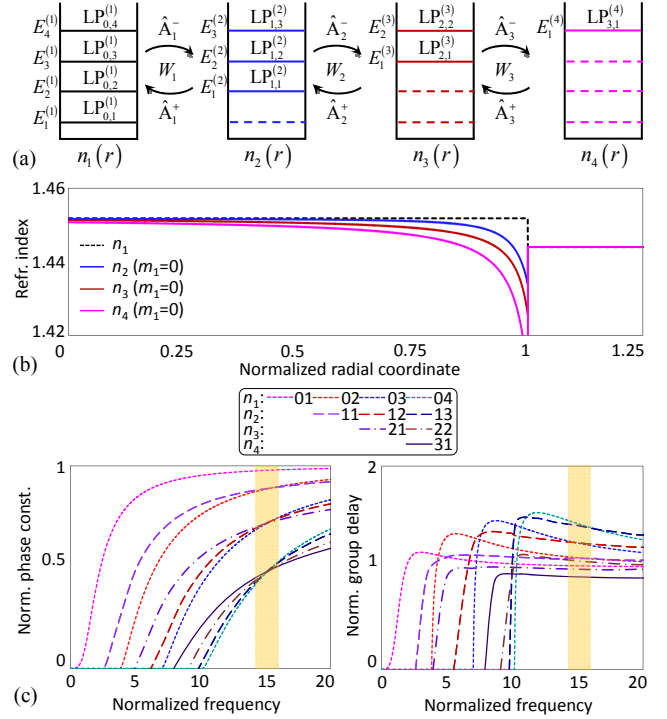
FIG. 4. Modal analysis of the unbroken SUSY Hamiltonian chain. (a) Symbolic representation of the SUSY chain. (b) Supersymmetric refractive indexes calculated from Eq. (19). (c) Normalized dispersion diagram and normalized group delay of the LP modes in the SUSY chain.

$$R_{m_1+q-1,n}^{(q)}(r) = \frac{\xi}{\sqrt{r}}\left(\prod_{i=1}^{q-1}\hat{A}_{q-i}^-\right)\left(\sqrt{r}R_{m_1,n+q-1}^{(1)}(r)\right), \quad (21)$$

where $\hat{A}_l^- := d/dr + W_l(r)$ and W_l is the superpotential connecting n_l and n_{l+1}. W_l can be calculated from the corresponding ground state of the l-th system $\psi_{ml,1}^{(l)}$ as $W_l(r) = -(\ln\psi_{ml,1}^{(l)}(r))'$.

As an example, we perform a modal analysis of an unbroken SUSY chain with $N = 4$ and $m_1 = 0$. The numerical results are shown in Fig. 4. All refractive index profiles are non-singular, thanks to the choice $m_l = m_1 + l - 1$ [see Fig. 4(b)]. As before, it can be theoretically shown that the bound states of each system in the chain are continuous normalizable eigenfunctions [49]. This is further confirmed through numerical simulations [Fig. 4(c)], which evidence that degeneracy is present throughout the whole chain (implicitly validating the application of step D and the SVI and paraxial approximations for all systems).

Although the PMBW is slightly reduced in the fourth system, the group delay of higher-order modes (specially the $LP_{3,1}^{(4)}$) is lower than that of the fundamental mode of the first system, the $LP_{0,1}^{(1)}$. This opens up the possibility of enabling privileged optical transmissions in higher-order LP modes. Moreover, the unexpected flexibility provided by SUSY in the design of exotic propagation properties
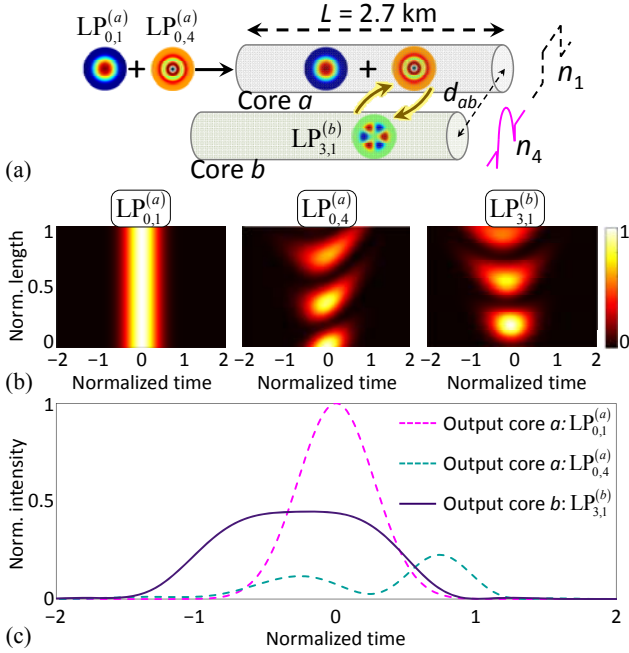
FIG. 5. (a) Pulse propagation in a 3-km 2-core SUSY MCF. (b) Simulation results of a 20-ns Gaussian optical pulse propagating through the MCF length when the $LP_{0,1}^{(a)}$ and $LP_{0,4}^{(a)}$ modes are stimulated at the MCF input (colorbar: normalized intensity). (c) Pulse shaping at the MCF output.

(such as weak dispersion or low group delay) can be combined with the mode-coupling phenomenon to design MCFs with special features for, e.g., mode conversion, mode filtering, dispersion engineering and pulse shaping.

In order to illustrate these potential applications, we perform a pulse propagation simulation using a beam propagation method (BPM) along a 2.7-km MCF comprising two cores a and b with $R_0 = 25$ μm, $\lambda_0 = 1550$ nm and index profiles $n_a = n_1$ and $n_b = n_4$. For simplicity, we employ the notation $LP_{m,n}^{(a)} \equiv LP_{m,n}^{(1)}$ and $LP_{m,n}^{(b)} \equiv LP_{m,n}^{(4)}$. The core-to-core distance d_{ab} (measured from the center of the cores) is fixed to 75 μm. A Gaussian optical pulse with a temporal width of 20-ns (at $1/2e$ of the peak intensity) excites the $LP_{0,1}^{(a)}$ and $LP_{0,4}^{(a)}$ modes with a peak power of 0 dBm in order to guarantee that we are operating in the linear regime of the MCF. For this value of peak power, the pulse distortion induced by the nonlinear effects of the optical medium can be neglected [51].

Figure 5 depicts the simulated pulse propagation for the $LP_{0,1}^{(a)}$, $LP_{0,4}^{(a)}$ and $LP_{3,1}^{(b)}$ modes. The time was normalized with respect to the group delay of the $LP_{0,1}^{(a)}$ mode $\tau_{G,01}^{(a)}$ as $t_N = (t - \tau_{G,01}^{(a)} \cdot z)/T_P$, where T_P is the full-width at $1/2e$ of the peak pulse power. The z-coordinate was normalized to the MCF length, i.e., $z_N = z/L$. Figure 5(b) shows that the pulse propagating through the $LP_{0,1}^{(a)}$ retains its shape along the MCF length as a direct consequence of the phase-mismatching of this mode, not

only with the $LP_{3,n}^{(b)}$ modes, but also with any $LP_{m,n}^{(b)}$ mode (it was numerically tested that $\beta_{0,1}^{(a)} > \beta_{m,n}^{(b)}$ at $\lambda_0 = 1550$ nm).

However, the shape of an optical pulse launched to the $LP_{0,4}^{(a)}$ mode is modified along the MCF due to the intermodal dispersion between the degenerate $LP_{0,4}^{(a)}$ and $LP_{3,1}^{(b)}$ modes [see Fig. 4(c)]. Figure 5(c) shows the pulse shape observed at the MCF output for each mode. As demonstrated in [51], the first-order intermodal dispersion between two different phase-matched LP core modes $[\delta b(\lambda_0) = 0]$ can be modeled by two linear and time-invariant systems with impulse response approximately proportional to $\delta(t - \Delta\tau_G \cdot z) + \delta(t + \Delta\tau_G \cdot z)$ in core a and $\delta(t - \Delta\tau_G \cdot z) - \delta(t + \Delta\tau_G \cdot z)$ in core b, where $\Delta\tau_G$ is the DMGD between the LP modes and $\delta(t)$ is the Dirac delta function. That is, the input pulse is transformed into the sum of two pulses with a relative delay of $2\Delta\tau_G \cdot L$ at the fiber output. In particular, the first-order intermodal dispersion length $L_{ID}^{(1)} = T_P/(2\Delta\tau_G)$ indicates the MCF length scales over which the dispersive effects of the first-order intermodal dispersion should be considered. Since $L > L_{ID}^{(1)} = 0.4$ km, the first-order intermodal dispersion between the $LP_{0,4}^{(a)}$ and $LP_{3,1}^{(b)}$ modes allows us to generate different pulse shapes by optimizing L. For instance, in the example of Fig. 5, L was chosen so that the two pulses into which the initial pulse launched into the $LP_{0,4}^{(a)}$ mode is transformed, add up to form a flat-top pulse with a broadened temporal width and a lower group delay than the original one. Likewise, note that the $LP_{0,1}^{(a)}$ mode is filtered at the output of the core a.

Along these same lines, it should be noted that the group-velocity dispersion (GVD) — also referred to as chromatic dispersion in the photonic literature — can be neglected in each LP mode. The GVD should only be considered in a given $LP_{m,n}$ mode when $L > L_{GVD} = T_P^2/\beta_{2,m,n}$, where $\beta_{2,m,n} = d^2\beta_{m,n}/d\omega^2$ [52]. Typically, $\beta_{2,m,n}$ is of the order of -20 ps²/km or lower in weakly-guiding silica fibers [51]−[53]. Thus, since $L << L_{GVD} \sim 2 \cdot 10^7$ km, we can neglect the pulse distortion induced by the GVD in Fig. 5(c).

The unbroken SUSY procedure and its intriguing features and applications can also be exploited by using planar waveguides [24]−[28]. In this context, a planar SUSY mode converter has been experimentally demonstrated in [28] by Heinrich et al. by performing a discrete representation of the refractive index profile using photonic lattices. In contrast to SUSY optical fibers, a SUSY mode converter with planar structure would be of special interest for signal processing applications in integrated photonics [54],[55]. However, the device demonstrated in Fig. 5 could be of extreme utility in applications requiring an all-fiber design, especially, for a fully integrated realization of angular momentum multiplexing [42]. Along this line, novel pulse shaping and dispersion management applications based on unbroken SUSY fiber chains can be explored within the framework of microwave photonics and radio-over-fiber

transmissions for the next-generation 5G cellular networks [56],[57]. Furthermore, note that in contrast to the classical mode conversion and mode filtering strategies based on rectangular waveguides and optical fibers with different width [39],[58]−[60], the unbroken SUSY procedure allows us to perform these functionalities in an extremely high optical bandwidth [see Figs. 2 and 4].

Moreover, the singular features of the unbroken SUSY chain allows us to design MCFs and selective photonic lanterns with unique broadband intra- and intermodal dispersion properties [Fig. 4(c)] that would be difficult to obtain with classical step-index or gradual-index profiles [61]−[66]. The concept of photonic lantern was originally conceived in the field of astrophotonics to couple the light between a multi-mode single-core fiber and individual single-mode single-core fibers [61]. In recent years, this device has been extensively developed to inject (extract) light to (from) optical fibers in space-division multiplexing transmissions (i.e., multiplexing techniques that establish multiple spatially distinguishable data paths using multi-mode single-core fibers [62]−[66] and MCFs [67]), as well as for other applications [68]. The photonic lanterns considered in these previous works (based on classical step-index and gradual-index profiles) support homogeneous supermodes, i.e., supermodes generated from the linear combination of degenerate LP modes with the same azimuthal and radial order. Typically, these supermodes are constructed through the linear combination of the LP_{01} mode of different cores in a MCF, which requires a high number of cores to obtain supermodes with large effective area [64]. This is of special interest to increase the tolerance of the signal-to-noise ratio to the fiber Kerr nonlinearities in space-division multiplexing systems. In such a scenario, the advantage of SUSY would be that it allows us to construct photonic lanterns with heterogeneous supermodes, generated from the linear combination of different LP mode groups. In this vein, supermodes with large effective area can be designed using a MCF with a reduced number of SUSY cores.

As a specific example, we designed a MCF comprising two cores a and b with $R_0 = 9$ μm, $d_{ab} = 2R_0$, $n_a = n_1$ and $n_b = n_2(m_1 = 0, \lambda_0 = 1550$ nm). Figures 6(a)-6(c) show the intensity mode profile $I(x,y)$ of different hybrid modes of the MCF calculated with the 3D mode solver of CST Microwave Studio at $\lambda_0 = 1550$ nm. As can be seen, this structure supports both isolated LP modes [Fig. 6(a) and 6(b)] and supermodes [Fig. 6(c)], depending on the stimulated hybrid modes. Remarkably, the supermode of Fig. 6(c) is generated in the MCF from the almost perfect phase-matching between LP modes of different azimuthal order ($LP_{0,2}^{(a)} \pm LP_{1,1}^{(b)}$ in this case). As a result, SUSY allows us to generate designer heterogeneous supermodes with large effective area $A_{eff} = (\iint I(x,y)dxdy)^2 / \iint I^2(x,y)dxdy$ in a high optical bandwidth and using only two cores [see Fig. 6(d)].
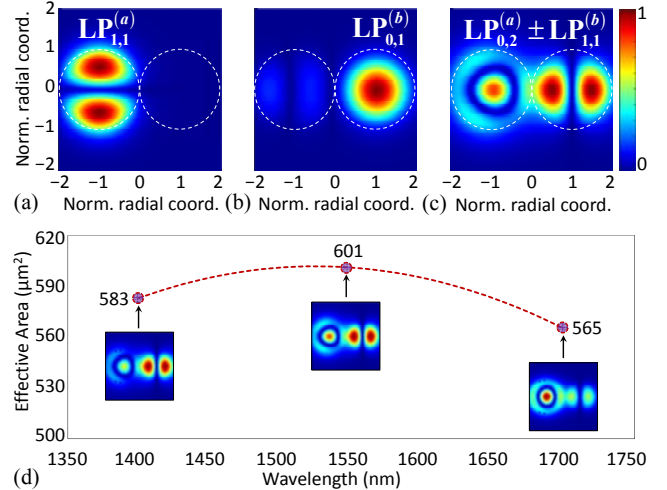
FIG. 6. Calculated intensity mode profiles of different hybrid modes of the SUSY coupled-core MCF at 1550 nm: (a) 6-th hybrid mode, (b) 8-th hybrid mode and (c) 15-th hybrid mode. (d) Effective area of the supermode $LP_{0,2}^{(a)} \pm LP_{1,1}^{(b)}$ as a function of the wavelength. Colorbar: normalized intensity.

B. Broken SUSY

Broken and isospectral (see next section) SUSY transformations relate the spectra of the original (V_1) and transformed potentials (V_2) through the relation $E_n^{(2)} = E_n^{(1)}$. In this way, we will be able to establish a perfect phase-matching between the $LP_{m_1,n}^{(1)}$ and $LP_{m_2,n}^{(2)}$ modes at λ_0, provided that the conditions for the degeneracy between the optical systems $[\mathcal{E}_{m1,n}^{(1)}, n_1]$ and $[\mathcal{E}_{m2,n}^{(2)}, n_2]$ are satisfied (see Section II). In such circumstances, mode conversion applications between LP modes with the same radial order could be explored by using the broken (and isospectral) SUSY procedure. On the other hand, if degeneracy were not preserved (which will turn out to be the case for the broken transformations analyzed in this section), the corresponding SUSY transformation could be employed as a mathematical strategy to design gradual-index MCFs with a high core density and a low mode-coupling between the LP modes of different cores (also termed in the literature as inter-core crosstalk) within a large bandwidth. Finally, a partial degeneracy (which will be the case for the isospectral constructions studied in next section) could be used to achieve unprecedented selective mode filtering configurations without mode conversion provided that $m_1 = m_2$.

The SUSY relation between V_1 and V_2 is spontaneously broken if $\alpha \neq E_1^{(1)}$. In this work, we focus on the case $\alpha < E_1^{(1)}$. Redefining the auxiliary constant as $\alpha \equiv -k^2 \cdot n_\alpha^2$, where $k = \omega/c_0$, we find that SUSY is broken if n_α is higher than the effective refractive index of the ground state $LP_{m1,1}^{(1)}$, i.e., $n_\alpha > \beta_{m1,1}^{(1)}/k$. The previous condition is

guaranteed by selecting $n_\alpha > \max\{n_1(r)\}$, in which case, the solution to Eq. (10) for the step-index profile is:

$$W(r) = iX(r)\left[\frac{J'_{m_1}(-irX(r)) + Y'_{m_1}(-irX(r))}{J_{m_1}(-irX(r)) + Y_{m_1}(-irX(r))}\right] - \frac{1}{2r}, \quad (22)$$

where $X(r) = (\omega/c_0)\cdot[n_\alpha^2 - n_1^2(r)]^{1/2}$. The index n_2 is calculated from the superpotential as:

$$n_2(r) = \sqrt{n_1^2(r) - 2\frac{c_0^2}{\omega^2}\frac{\mathrm{d}}{\mathrm{d}r}\left(\frac{m_2^2 - m_1^2}{2r} + W(r)\right)}. \quad (23)$$

As in the previous section, $W(r)$ is found to be singular. However, $W(r)$ and n_2 are now complex functions. This means that n_2 includes local gain or loss (via its imaginary part), as in some transformation optics approaches [69]−[71].

Let us analyze under which conditions n_2 will be non-singular, depending on the relation between m_1 and m_2:

- $m_1 = m_2$: n_2 will not be singular only for a non-singular $W(r)$, which cannot be the case.
- $m_1 < m_2$: n_2 is bounded at $r = 0$ if $W(r\to0) = -\infty$. Nevertheless, from Eq. (22), $W(r\to0) = +\infty$.
- $m_1 > m_2$: As $W(r\to0) \propto (2m_1-1)/2r$ when $m_1 > 0$, n_2 becomes non-singular if $m_2 = m_1-1$.

Thus, we focus on the last case in what follows. A particular example with $m_1 = 2$, $m_2 = 1$, $\lambda_0 = 1550$ nm, and $n_\alpha = 1.452$ is considered. In this case, in order to simulate a complex refractive index profile, we use the 3D electromagnetic mode solver of COMSOL. Figures 7(a) and 7(b) depict the real (blue line) and imaginary (red line) parts of the broken SUSY index n_2 and W. As expected, W presents a singularity at $r = 0$, but n_2 is non-singular. Surprisingly, in this case both optical systems are found to be non-degenerate concerning the SUSY modes $\mathrm{LP}_{m1,n}^{(1)}$ and $\mathrm{LP}_{m2,n}^{(2)}$ [Fig. 7(c)]. Nonetheless, as can be seen from Fig. S4 in [49], additional LP modes are found to be degenerate at different frequencies in the third transmission optical window (normalized frequency between 14.2 and 16). Furthermore, the imaginary part of n_2 induces at 1550 nm a mode-dependent loss per unit of length of 1.46 Np/m, 1.34 Np/m and 1.07 Np/m for the $\mathrm{LP}_{1,1}^{(2)}$, $\mathrm{LP}_{1,2}^{(2)}$ and $\mathrm{LP}_{1,3}^{(2)}$ modes, respectively [1 Np $\equiv$ 10log(e) dB $\approx$ 4.34 dB].

We investigated the different possible origins for the non-degeneracy between $[\mathcal{E}_{m1,n}^{(1)}, n_1]$ and $[\mathcal{E}_{m2,n}^{(2)}, n_2]$. Firstly, we verified that the singularity of W involved in step C is not behind this unusual behavior, since the SUSY bound states $\psi_{m2,n}^{(2)} \propto \hat{A}^-\psi_{m1,n}^{(1)}$ are again continuous normalizable solutions [49]. Then, we checked whether the absence of degeneracy may come from a violation of the optical boundary condition at $r = 0$ by the SUSY modes of $V_2^{(3D)}$ after step D. This is not the case either, since $R_{m2,n}^{(2)}(0) = 0$ in the analyzed case [49]. By process of elimination, the non-degeneracy must be induced by step E. In fact, although we found that the SVI criterion is fulfilled
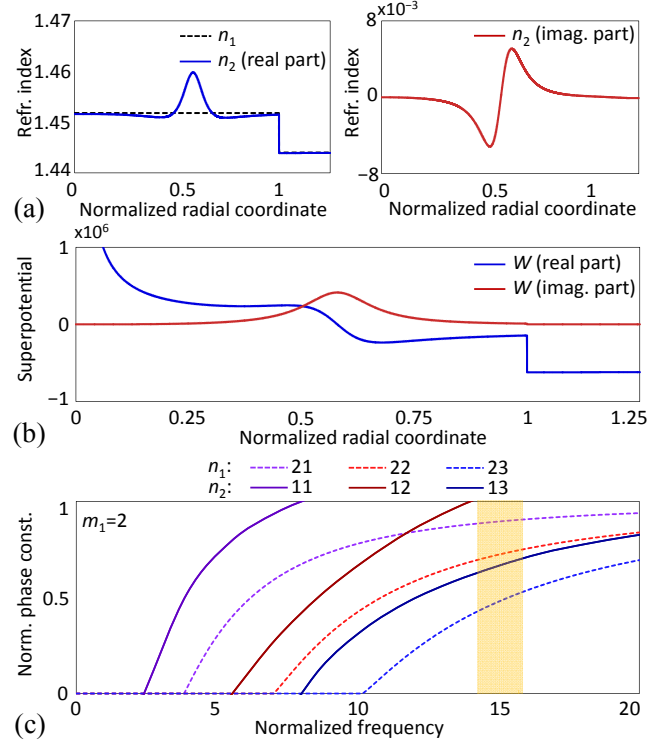
FIG. 7. Broken SUSY 1D. (a) SUSY partner for the step-index profile, (b) superpotential (blue line: real part, red line: imaginary part), and (c) normalized dispersion diagram of the broken SUSY pattern of the step-index profile assuming $m_1 = 2$ and $m_2 = 1$ in Eq. (23).

($\delta n_2 \leq 0.01 \ll n_2$ in $\delta r \sim n_2\lambda_0$), the paraxial approximation is strongly degraded for $V_2^{(3D)}(r)$. Specifically, we verified that the true modes of the n_2 profile are quasi-LP modes [72] and, as analyzed in the supplemental material, while the true modes are quasi-degenerate, their longitudinal component $\mathcal{E}_z$ cannot be neglected with respect to the transversal one $\mathcal{E}_\mathrm{T}$ ($\mathcal{E}_z/\mathcal{E}_\mathrm{T} \approx 0.1$). Therefore, as the eigenmodes of $V_2^{(3D)}$ do not approximately satisfy Eq. (2), the degeneracy between both spectra is broken.

This exclusive feature of broken SUSY in axially-symmetric optical media can be used to design MCFs with a high density of cores propagating non-degenerate modes with low inter-core crosstalk levels. The ever-decreasing core-to-core distance in MCFs (aiming at increasing the core density and hence the channel capacity) significantly enhances the inter-core crosstalk levels [73]. In this scenario, gradual-index MCFs comprising a high core density with low inter-core crosstalk levels can be designed with the broken 1D SUSY procedure. In [49] we also analyze additional strategies as the inverse SUSY transformation.

On the other hand, note that in all the analyzed SUSY transformations $\alpha \leq E_1^{(1)}$. The reason for not having

discussed the $\alpha > E_1^{(1)}$ case is that it is related to a superpotential $W^{(n)}(r) = -(\ln \psi_{m1,n}^{(1)}(r))'$, where $n > 1$ and $\psi_{m1,n}^{(1)}$ is a wave function with n nodes. Therefore, $W^{(n)}$ and V_2 will have $n-1$ singularities at $r > 0$ in this case, and so will the corresponding SUSY refractive index. Nevertheless, a superpotential $W^{(n)}$ could be an interesting alternative in complex cylindrical potentials with discrete spectrum and parity-time symmetry (e.g. to remove arbitrary modes [25]) or with continuum spectrum (e.g. to generate bound states in the continuum [74]).

IV. ISOSPECTRAL POTENTIALS

In the context of quantum mechanics, it is well-known that one can start from a given 1D potential and use SUSY transformations to construct single- and multi-parameter families of isospectral potentials, i.e., potentials with the same energy levels as the original one [14]. In this section, we investigate the application of these isospectral transformations to axially-symmetric optical potentials. As we will demonstrate, such transformations provide a privileged procedure to construct families of refractive index distributions supporting degenerate LP modes with a dimension-independent design control over their group delay. Furthermore, as mentioned above, selective mode filtering may also be performed if degeneracy is only partially preserved.

There exist different approaches to construct a single-parameter family [14]. For its intuitive character, we use here the so-called Darboux procedure, schematically depicted in Fig. 8(a) for the one-parameter case. In essence, it consists of first deleting the ground state $\psi_{m1,1}^{(1)}$ of V_1 with an unbroken SUSY transformation, obtaining the potential V_2. Remarkably, V_2 has a non-normalizable solution Φ_1 with energy $E_1^{(1)}$ that for axially-symmetric potentials takes the form [49]:

$$\Phi_1(r;\eta_1) = \frac{\mathcal{P}_1(r)+\eta_1}{\sqrt{r} R_{m_1,1}^{(1)}(r)}; \quad \mathcal{P}_1(r) = \int^r \tau \left(R_{m_1,1}^{(1)} \right)^2 (\tau) d\tau. \quad (24)$$

In a second step, we apply another unbroken SUSY transformation to V_2, taking Φ_1 as a virtual ground state, i.e., by using the superpotential:

$$W_D(r;\eta_1) = -\frac{d}{dr} \ln \Phi_1(r;\eta_1). \quad (25)$$

The resulting partner potential $\tilde{V}_1(r;\eta_1)$ will have a solution $1/\Phi_1$ at $E_1^{(1)}$, which will be normalizable if and only if $\eta_1 > 0$ or $\eta_1 < -\mathcal{P}_1(r\to\infty)$ [49]. In this case, a ground state of energy $E_1^{(1)}$ is reinserted, and we obtain the sought isospectral family $\tilde{V}_1(r;\eta_1)$ of $V_1(r)$. The corresponding refractive index profiles $\tilde{n}_1(r;\eta_1)$ and ground state functions $\tilde{R}_{m_1,1}^{(1)}(r;\eta_1)$ are [49]:

(a) $\tilde{V}_1(r;\eta_1)$

(b)

(c)
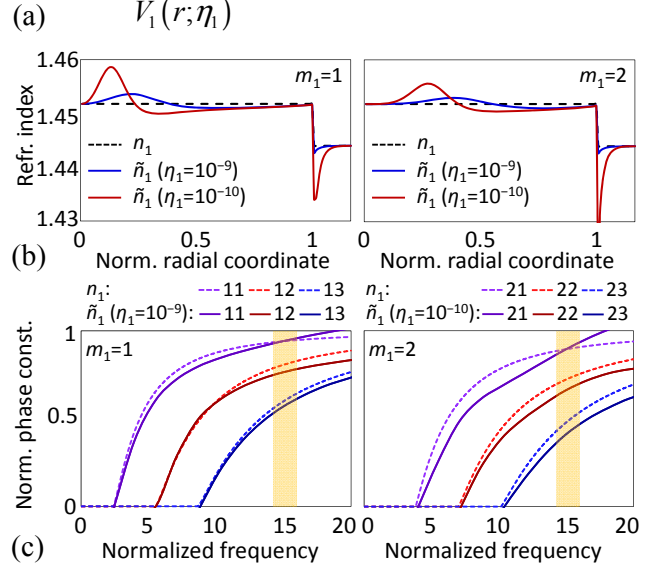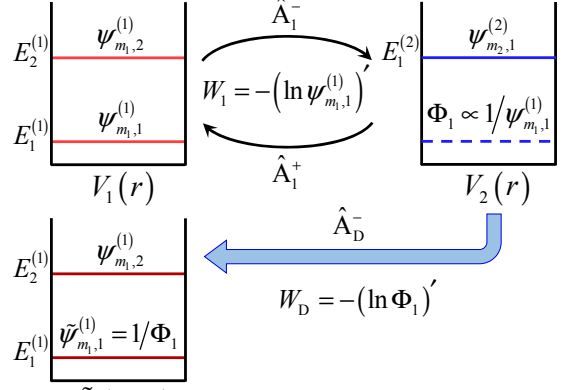
FIG. 8. One-parameter isospectral cylindrical potentials. (a) Flowchart of the Darboux procedure. (b) Isospectral refractive indexes. (c) Normalized diagram dispersion.

$$\tilde{n}_1(r;\eta_1) = \sqrt{n_1^2(r) + 2\frac{c_0^2}{\omega^2}\frac{d^2}{dr^2}\ln(\mathcal{P}_1(r)+\eta_1)}; \quad (26)$$

$$\tilde{R}_{m_1,1}^{(1)}(r;\eta_1) = R_{m_1,1}^{(1)}(r) / \mathcal{P}_1(r)+\eta_1. \quad (27)$$

Note that the Darboux procedure also involves a singular superpotential $W_D(\eta_1)$ [49]. In order to elucidate whether degeneracy is preserved in this isospectral construction, we study the cases $m_1 = 1$ and $m_1 = 2$ for two different values of η_1 (we include additional examples with different m_1 and η_1 values in Fig. S5 of [49]). The resulting profiles for $\tilde{n}_1$ are shown in Fig. 8(b). A closer look at the dispersion diagram (calculated with the 3D mode solver of CST Microwave Studio) for the cases $\tilde{n}_1(m_1=1,\eta_1=10^{-9})$ and $\tilde{n}_1(m_1=2,\eta_1=10^{-10})$ reveals an interesting unexpected result [Fig. 8(c)]: the Darboux procedure gives rise to optical media for which only the ground states of the selected isospectral family are degenerate. As in the broken SUSY

case, we found that this occurs as a result of a degradation of the paraxial approximation (step E). In particular, only the ground state of $\tilde{n}_1(r;\eta_1)$ satisfies that $\mathcal{E}_z \ll \mathcal{E}_T$, with $\mathcal{E}_z/\mathcal{E}_T \sim 0.01$. In contrast, the remaining bound states are found to be quasi-LP modes, with $\mathcal{E}_z/\mathcal{E}_T \sim 0.1$. A further description of the LP and quasi-LP modes of Fig. 8(c) can be found in [49].

In contrast to the classical mode filtering strategies based on using optical waveguides with different width [39],[58]−[60], and the unbroken SUSY procedure, this unique property allows us to perform a *true* mode (de)multiplexing of any (fundamental) $LP_{m1,1}$ mode, i.e., without having mode conversion between optical waveguides. A second advantage of the proposed isospectral construction is that the slope of the normalized propagation constant b associated with $\tilde{R}^{(1)}_{m_1,1}$ increases as η_1 tends to 0 (see Fig. 8(c) and Fig. S5 in [49]). Consequently, we have full control over the group delay of the SUSY ground state through this free parameter. These singular features open new paths for mode filtering, dispersion engineering and pulse shaping applications in photonics.

Aimed to illustrate the power of this method, we propose an all-fiber mode demultiplexer (M-DEMUX) of the first three LP mode groups ($LP_{0,1}$, $LP_{1,1}$ and $LP_{2,1}$) based on the presented theory. The M-DEMUX is designed using a 60-cm MCF comprising three cores a, b and c with a core-to-core distance $d_{ab} = d_{ac} = 55$ µm, $R_0 = 25$ µm, and $\lambda_0 = 1550$ nm [Fig. 9(a)]. The index profiles of cores a and c are calculated from Eq. (26) as $n_a = \tilde{n}_1(m_1=1,\eta_1=10^{-9})$ and $n_c = \tilde{n}_1(m_1=2,\eta_1=10^{-10})$. The index profile of core b is taken to be the previous step-index profile, with $n_b = n_1$. A 10-ps Gaussian optical pulse is launched to the LP_{01}, LP_{11} and LP_{21} modes of the central core, core b, with a peak power of 0 dBm to operate in the linear regime of the M-DEMUX. Figure 9(b) shows the BPM numerical results for the optical pulse propagating through each LP mode in the M-DEMUX. The time and length were normalized with respect to the group delay of the $LP_{0,1}^{(b)}$ mode and the MCF length, respectively. As desired, at the device output, the pulse launched into the $LP_{1,1}^{(b)}$ mode has hoped to the $LP_{1,1}^{(a)}$ mode, the pulse launched into the $LP_{0,1}^{(b)}$ mode remains at core b, and the pulse launched into the $LP_{2,1}^{(b)}$ mode has been transferred to the $LP_{2,1}^{(c)}$ mode.

In addition, Fig. 9(c) shows that, in this case, the modification of the pulse shape induced by the first-order intermodal dispersion of the M-DEMUX (i.e. the pulse dispersion) is quite low given that the length of the M-DEMUX is of the order of the first-order intermodal dispersion length, which is found to be $L_{ID}^{(1)} \approx 1.4$ m and 0.3 m between the $LP_{1,1}^{(a)}$-$LP_{1,1}^{(b)}$ and $LP_{2,1}^{(c)}$-$LP_{2,1}^{(b)}$ modes, respectively. As a result, a true modal demultiplexing (or modal multiplexing considering the reciprocal nature of the device) with a reduced pulse dispersion is demonstrated.
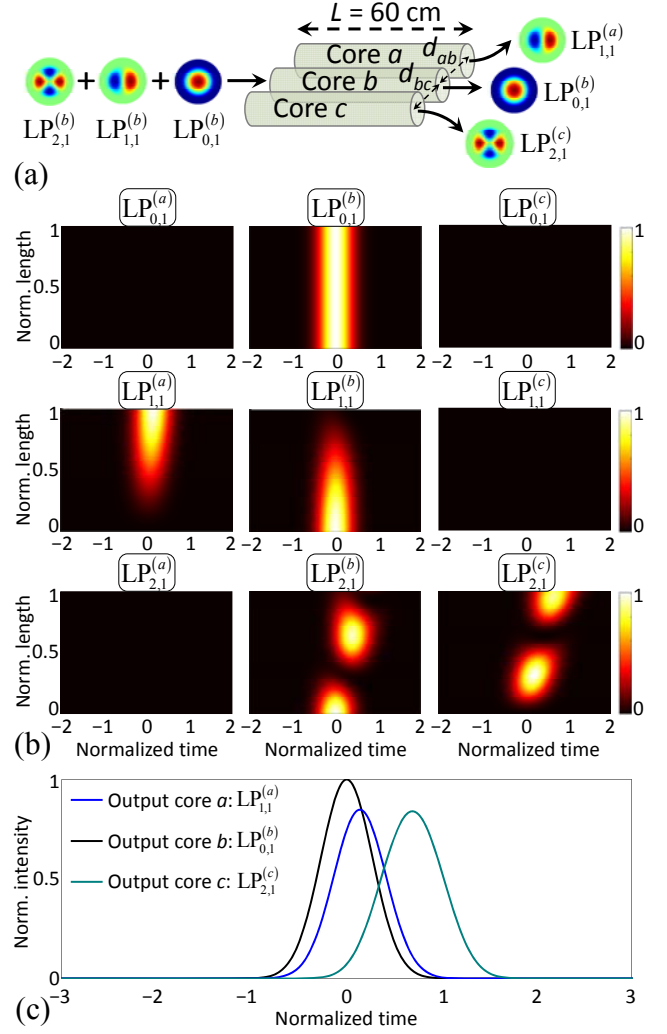
FIG. 9. M-DEMUX based on a 3-core MCF. (a) Schematic structure of the device with $n_a = \tilde{n}_1(m_1=1,\eta_1=10^{-9})$, $n_b = n_1$ and $n_c = \tilde{n}_1(m_1=2,\eta_1=10^{-10})$. (b) 10-ps Gaussian optical pulse propagating through the: LP_{01}, LP_{11} and LP_{21} modes of cores a, b and c (colorbar: normalized intensity). (c) Optical pulse at the M-DEMUX output.

Nonetheless, in contrast with the unbroken SUSY case (see Fig. 5), the Darboux procedure allows us to engineer the first-order intermodal dispersion of a MCF just by adjusting η_1. This provides us with a much higher design flexibility, as we can tailor this parameter even for fixed MCF length, core-to-core distance and core diameters. In this fashion, pulse shaping and dispersion engineering functionalities can be incorporated to the M-DEMUX. As an example, Fig. 10 depicts the behavior of the M-DEMUX now taking $\eta_1=10^{-11}$ for the cores a and c. These values were chosen so as to increase the intermodal dispersion with respect to the previous case and produce broadened and flat-top pulses at the M-DEMUX output. [Fig. 10(b)].
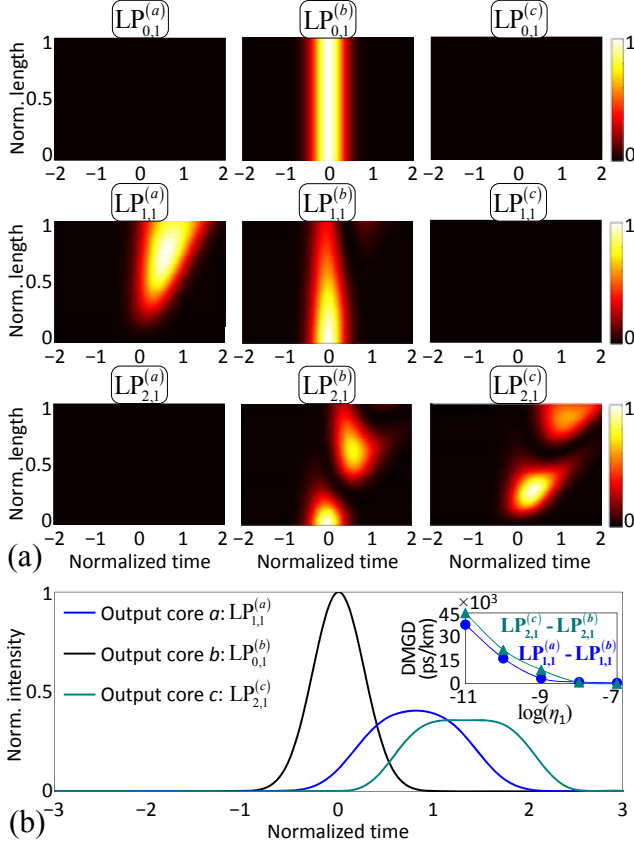
FIG. 10. (a) 10-ps Gaussian pulse propagating through the LP$_{01}$, LP$_{11}$ and LP$_{21}$ modes of the M-DEMUX with $n_a = \tilde{n}_1(m_1=1,\eta_1=10^{-11})$, $n_b = n_1$ and $n_c = \tilde{n}_1(m_1=2,\eta_1=10^{-11})$ (colorbar: normalized intensity). (b) Pulse shaping at the M-DEMUX output. The inset shows the DMGD between the LP$_{2,1}^{(c)}$-LP$_{2,1}^{(b)}$ modes and between the LP$_{1,1}^{(a)}$-LP$_{1,1}^{(b)}$ modes as a function of η_1.

Now, we found that $L_{\mathrm{ID}}^{(1)} \approx 0.14$ m and 0.11 m between the LP$_{1,1}^{(a)}$-LP$_{1,1}^{(b)}$ and LP$_{2,1}^{(c)}$-LP$_{2,1}^{(b)}$ modes, respectively.

Moreover, since the M-DEMUX length is much lower than the GVD length in the LP$_{0,1}$, LP$_{1,1}$ and LP$_{2,1}$ modes of each core ($L_{\mathrm{GVD}} \sim 5$ km), the pulse dispersion induced by the GVD can be neglected when propagating optical pulses in the picosecond regime (or higher temporal widths) in our M-DEMUX.

Because of the partial degeneracy observed in the one-parameter isospectral family, novel photonic devices can be designed for next-generation optical networks based on mode-division multiplexing (MDM) transmissions. In spite of the fact that the proposed M-DEMUX is not scalable to a higher number of modes if the number of cores (three in this case) is kept constant, we can achieve such a scalability by including additional adjacent cores around core b and optimizing the MCF length to extract higher-order modes from this core, e.g., the LP$_{3,1}$ and LP$_{4,1}$ modes. As an important example, an all-fiber add-drop mode multiplexer can be designed by using a MCF with a

hexagonal close-packed structure [62] along with isospectral constructions. In this way, the surrounding cores will inject and extract the LP$_{m,1}$ modes from the central core (at the corresponding λ_0 wavelength), which can be used to distribute the different multiplexed signals in the MDM system.

In addition, the Darboux procedure can also be generalized to obtain a n-parameter isospectral family of cylindrical potentials. In [49] we investigate the multi-parameter case and include an illustrative example of the two-parameter family for the step-index profile.

V. CONCLUDING REMARKS

In this paper we have applied different 1D SUSY variants to cylindrical optical potentials exhibiting axial symmetry. As SUSY transformations involve inverse-square 1D potentials and singular superpotentials, we investigated numerically and theoretically whether these features may produce a degeneracy between the corresponding 3D optical superpartners. Our results show that, while degeneracy is present in unbroken SUSY transformations, it is indeed violated in broken and isospectral SUSY transformations. Notably, this violation does not occur due to the aforementioned reasons, but it is actually induced at the energy levels for which the bound states of the SUSY optical medium do not satisfy the paraxial approximation. These results provide us with a recipe to construct axially-symmetric potentials with total, partial, or no degeneracy using unbroken, isospectral, or broken SUSY, respectively. Outstandingly, the unbroken and isospectral SUSY transformations share an extremely large phase-matching bandwidth.

Building on these interesting modal properties of optical superpartners, we have proposed and demonstrated a variety of applications for mode filtering, mode conversion, mode multiplexing, supermode generation, pulse shaping and dispersion engineering. These include SUSY multi-core fibers, mode-selective photonic lanterns and true all-fiber modal (de)multiplexers. Specifically, the true mode (de)multiplexer is designed using optical potentials with partial degeneracy induced by the violation of the paraxial approximation. Remarkably, this concept has not been previously observed in the optical SUSY literature [23]−[29]. In this vein, these results could be extrapolated to SUSY planar waveguides, which may open new possibilities for signal processing applications in integrated photonics [54],[55].

The SUSY transformation method depicted in Fig. 1 can be generalized by analyzing additional factorization procedures of the SUSY Hamiltonian given by Eq. (11) [75],[76]. As such, SUSY fiber transformations can likewise be employed to study new degenerate axially-symmetric potentials with a different azimuthal relation from those for the unbroken and broken SUSY cases. The

TABLE I. Physical interpretation of the eigenvalue, potential and wave function of Eq. (2) in photonics, quantum mechanics and acoustics. The speed of light in a vacuum is denoted as c_0, while c_s represents the speed of sound.

	$E_{m,n}^{(3D)}$	$V^{(3D)}(r)$	$\Psi_{m,n}(\mathbf{r})$
Photonics	0	$-\dfrac{\omega^2}{c_0^2}n^2(r)$	$\mathcal{E}_{m,n}(\mathbf{r},\omega)$ $\mathcal{H}_{m,n}(\mathbf{r},\omega)$
Quantum Mechanics	$\tilde{E}_{m,n}$	$\tilde{V}(r)$	$\tilde{\psi}_{m,n}(\mathbf{r})$
Acoustics	0	$-\dfrac{\omega^2}{c_s^2(r)}$	$\phi_{m,n}(\mathbf{r},\omega)$ $P_{m,n}(\mathbf{r},\omega)$

proposed idea builds a bridge to investigate novel mode conversion and mode filtering strategies in all-fiber devices.

On the other hand, it is worth mentioning the possibility of extrapolating the proposed transformation method to acoustics and quantum mechanics when axially-symmetric potentials are involved. Interestingly, Eq. (2) serves as a master equation that allows us to describe the dynamics of waves in these branches of physics, provided that an adequate mathematical identification of $E_{m,n}^{(3D)}$, $V^{(3D)}(r)$ and $\Psi_{m,n}(\mathbf{r})$ is performed. We include in Table I a possible choice of the physical meaning of these parameters in each of the aforementioned fields [other options are accounted for by introducing a free-parameter in $E_{m,n}^{(3D)}$ and $V^{(3D)}(r)$ for the photonic and acoustic cases, e.g., $E_{m,n}^{(3D)} \equiv \gamma$ and $V^{(3D)}(r) \equiv \gamma - (\omega^2/c_0^2)n(r)$]. In quantum mechanics, the wave equation is given by the time-independent Schrödinger equation. Hence, $E_{m,n}^{(3D)}$, $V^{(3D)}(r)$ and $\Psi_{m,n}(\mathbf{r})$ describe respectively the particle's discrete energy levels, the quantum potential, and the probability amplitude. Moreover, Eq. (2) models the propagation of sound in acoustic media with slowly-varying mass density, provided that we use the identifications of the third column of Table I. In this case, $\Psi_{m,n}(\mathbf{r})$ may represent the acoustic velocity potential or the acoustic pressure [77].

The applicability of 1D SUSY in these fields is straightforward by employing Table I and Eqs. (7), (8). Given that the degeneracy between $V_1^{(3D)}$ and $V_2^{(3D)}$ is present in all the analyzed cases (unbroken, broken and isospectral deformations) [49], one would expect the same behavior for the case in which $V_1^{(3D)}$ and $V_2^{(3D)}$ represent acoustic or quantum systems, as they involve no paraxial approximations. However, this should be confirmed through further numerical analyses. If degeneracy is indeed preserved, our results for unbroken SUSY can be directly extrapolated to these fields. Hence, multi-core acoustic ducts or cylindrical quantum potentials with axial symmetry may be engineered with the same modal properties as unbroken SUSY MCFs. Furthermore, it would be interesting to explore broken SUSY transformations within the context of quantum mechanics as a theoretical

procedure to generate complex $V_2^{(3D)}$ potentials from a given $V_1^{(3D)}$ real analytically solvable potential. This may present interesting practical applications in Bose-Einstein condensates (BEC) [78]. Finally, proceeding in a similar manner as in Section IV, isospectral deformations may also be proposed as a strategy to construct acoustic and quantum axially-symmetric potentials with similar spectra.

ACKNOWLEDGEMENTS

[1] Y. A. Gol'fand and E. P. Likhtman, Extension of the algebra of Poincare group generators and violation of P invariance, JETP Lett. **13**, 452 (1971).

[2] P. Ramond, Dual theory for free fermions, Phys. Rev. D **3**, 2415 (1971).

[3] A. Neveu and J. H. Schwarz, Factorizable dual model of pions, Nucl. Phys. B **31**, 86 (1971).

[4] J. Wess and B. Zumino, Supergauge transformations in four dimensions, Nucl. Phys. B **70**, 39 (1974).

[5] D. Z. Freedman, P. van Nieuwenhuizen and S. Ferrara, Progress toward a theory of supergravity, Phys. Rev. D **13**, 3214 (1976).

[6] E. Witten, Dynamical breaking of supersymmetry, Nucl. Phys. B **188**, 513 (1981).

[7] E. Witten, Constraints on supersymmetry breaking, Nucl. Phys. B **202**, 253 (1982).

[8] M. B. Green, J. Schwarz, and E. Witten, *Superstring Theory* (Cambridge University Press, Cambridge, U.K., 1987).

[9] F. Takayama and M. Yamaguchi, Gravitino dark matter without R-parity, Phys. Lett. B **485**, 388 (2000).

[10] H. Goldberg, Constrain on the photino mass from cosmology, Phys. Rev. Lett. **50**, 1419 (1983).

[11] M. Hirsch, W. Porod, and D. Restrepo, Collider signals of gravitino dark matter in bilinearly broken R-parity, JHEP **03**, 062 (2005).

[12] L. M. Krauss, New constraints on 'INO' masses from cosmology (I). Supersymmetric 'inos', Nucl. Phys. B **227**, 556 (1983).

[13] K. A. Ulmer, Supersymmetry: experimental status, arXiv:1601.03774.

[14] F. Cooper, A. Khare and U. Sukhatme, Supersymmetry and quantum mechanics, Phys. Rep. **251**, 267 (1995).

[15] A. A. Andrianov and M. V. Ioffe, Nonlinear supersymmetric quantum mechanics: concepts and realizations, arXiv:1207.6799.

[16] B. Bagchi, F. Cannata, and C. Quesne, PT-symmetric sextic potentials, Physics Letters A **269**, 79 (2000).

[17] M. Znojil, F. Cannata, B. Bagchi, and R. Roychoudhury, Supersymmetry without hermiticity within PT symmetric quantum mechanics, Physics Letters B **483**, 284 (2000).

[18] F. Cannata, M. Ioffe, R. Roychoudhury, and P. Roy, A new class of PT-symmetric Hamiltonians with real spectra, Physics Letters A **281**, 305 (2001).

[19] B. F. Samsonov, Spectral singularities of non-Hermitian Hamiltonians and SUSY transformations, J. Phys. A **38**, L571 (2005).

[20] J. Bai and D. Citrin, Supersymmetric optimization of second-harmonic generation in mid-infrared quantum cascade lasers, Opt. Express **14**, 4043 (2006).

[21] E. M. C. Abreu, M. A. De Andrade, L. P. G. De Assis, J. A. Helayël-Neto, A. L. M. A. Nogueira, and R. C. Paschoal, A supersymmetric model for graphene, JHEP **05**, 001 (2011).

[22] A. del Campo, M. G. Boshier, and A. Saxena, Bent waveguides for matter-waves: supersymmetric potentials and reflectionless geometries, Sci. Rep **4**, 5274 (2014).

[23] S. M. Chumakov and K. B. Wolf, Supersymmetry in Helmholtz optics, Phys. Lett. A **193**, 51 (1994).

[24] M.-A. Miri, M. Heinrich, R. El-Ganainy, and D. N. Christodoulides, Supersymmetric optical structures, Phys. Rev. Lett. **110**, 233902 (2013).

[25] M.-A. Miri, M. Heinrich, and D. N. Christodoulides, Supersymmetry-generated complex optical potentials with real spectra, Phys. Rev. A **87**, 043819 (2013).

[26] H. P. Laba and V. M. Tkachuk, Quantum-mechanical analogy and supersymmetry of electromagnetic wave modes in planar waveguides, Phys. Rev. A **89**, 033826 (2014).

[27] M.-A. Miri, M. Heinrich, and D. N. Christodoulides, SUSY-inspired one-dimensional transformation optics, Optica **1**, 89 (2014).

[28] M. Heinrich, M.-A. Miri, S. Stützer, R. El-Ganainy, S. Nolte, A. Szameit, and D. N. Christodoulides, Supersymmetric mode converters, Nat. Comm. **5**, 3698 (2014).

[29] B. Midya, Supersymmetry-generated one-way-invisible PT-symmetric optical crystals, Phys. Rev. A **89**, 032116 (2014).

[30] T. D. Imbo and U. P. Sukhatme, Supersymmetric quantum mechanics and large-N expansions, Phys. Rev. Lett. **54**, 2184 (1985).

[31] F. Buonocore, G. Iadonisi, D. Ninno, and F. Ventriglia, Polarons in cylindrical quantum wires, Phys. Rev. B **65**, 205415 (2002).

[32] D. C. Dillen, K. Kim, E.-S. Liu and E. Tutuc, Radial modulation doping in core-shell nanowires, Nat. Nanotech. **9**, 116 (2014).

[33] H. Esfahlani, H. Lissek, and J. R. Mosig, Generation of acoustic helical wavefronts using metasurfaces, Phys. Rev. B **95**, 024312 (2017).

[34] E. J. Brambley and N. Peake, Classification of aeroacoustically relevant surface modes in cylindrical lined ducts, Wave Motion **43**, 301 (2006).

[35] S. W. Rienstra, A classification of duct modes based on surface waves, Wave Motion **37**, 119 (2003).

[36] H. Rämmal and J. Lavrentjev, Sound Reflection at an Open End of a Circular Duct Exhausting Hot Gas, Noise Control Eng. Journal **56**, 107 (2008).

[37] D. Gloge, Weakly guiding fibers, Applied Optics **10**, 2252 (1971).

[38] R.G.H. van Uden, R. A. Correa, E.A. López, F.M. Huijskens, C. Xia, G. Li, A. Schülzgen, H. de Waardt, A.M.J. Koonen, and C.M. Okonkwo, Ultra-high-density spatial division multiplexing with a few-mode multi-core fibre, Nat. Phot. **8**, 865 (2014).

[39] J. L. Corral, D. G.-Rodríguez, and R. Llorente, Mode-selective couplers for two-mode transmission at 850 nm in standard SMF, IEEE Phot. Tech. Lett. **28**, 425 (2016).

[40] T.-Y. Kao, J. L. Reno, and Q. Hu, Phase-locked laser arrays through global antenna mutual coupling, Nat. Phot. **10**, 541 (2016).

[41] B. E. A. Saleh and M. C. Teich, *Fundamentals of Photonics* (Wiley, 2007).

[42] J. Wang, J.Y. Yang, I. M. Fazal, N. Ahmed, Y. Yan, H. Huang, Y. Ren, Y. Yue, S. Dolinar, M. Tur, and A. E. Willner, Terabit free-space data transmission employing orbital angular momentum multiplexing, Nat. Phot. **6**, 488 (2012).

[43] A. Jevicki and J. Rodrigues, Singular potentials and supersymmetry breaking, Phys. Lett. B **146**, 55 (1984).

[44] M. Shifman, A. Smilga, and A. Vainshtein, On the Hilbert space of supersymmetric quantum systems, Nucl. Phys. B **299**, 79 (1988).

[45] P. Roy and R. Roychoudhury, Question of degenerate states in supersymmetric quantum mechanics, Phys. Rev. D **32**, 1597 (1985).

[46] P. K. Panigrahi, Singular superpotentials in supersymmetric quantum mechanics, Phys. Lett. A **178**, 251 (1993).

[47] W. M. Frank, D. J. Land, and R. M. Spector, Singular potentials, Rev. Mod. Phys. **43**(1), 36 (1971).

[48] A. Gangopadhyaya, P. K. Panigrahi and U. P. Sukhatme, Analysis of inverse-square potentials using supersymmetric quantum mechanics, J. Phys. A: Math. Gen. **27**, 4295 (1994).

[49] See Supplemental Material for additional theoretical discussions and numerical examples of supersymmetric transformations in optical fibers.

[50] D. W. Peckham, Y. Sun, A. McCurdy, and R. Lingle, *Optical Fiber Telecommunications VIA: Components and Subsystems*, edited by I. P. Kaminow, T. Li and A. E. Willner, (Elsevier, 2013), Chap. 8.

[51] A. Macho, C. García-Meca, F. J. Fraile-Peláez, F. Cortés-Juan, and Roberto Llorente, Ultra-short pulse propagation model for multi-core fibers based on local modes, Scientific Reports **7**, 16457 (2017).

[52] G. P. Agrawal, *Nonlinear Fiber Optics* (Elsevier Academic Press, Oxford, U.K., 2013).

[53] S. Mumtaz, R. J. Essiambre, and G. P. Agrawal, Nonlinear propagation in multimode and multicore fibers: generalization of the Manakov equations, J. Lightwave Techn. **31**, 398 (2013).

[54] C. García-Meca, S. Lechago, A. Brimont, A. Griol, S. Mas, L. Sánchez, L. Bellieres, N. S. Losilla, and J. Martí, On-chip wireless silicon photonics: from reconfigurable interconnects to lab-on-chip devices, Light: Science&Applications **6**, e17053 (2017).

[55] D. Pérez, I. Gasulla, L. Crudgington, D. J. Thomson, A. Z. Khokhar, K. Li, W. Cao, G. Z. Mashanovich, and J. Capmany, Multipurpose silicon photonics signal processor core, Nat. Comm. **8**, 636 (2017).

[56] I. Gasulla and J. Capmany, Microwave photonics applications of multicore fibers, IEEE Photonics Journal **4**, 877 (2012).

[57] A. Macho, M. Morant, and R. Llorente, Next-generation optical fronthaul systems using multicore fiber media, J. Lightwave Techn. **34**, 4819 (2016).

[58] K. Y. Song, I. K. Hwang, S. H. Yun, and B. Y. Kim, High performance fused-type mode-selective coupler using elliptical core two-mode fiber at 1550 nm, IEEE Photon. Technol. Lett. **14**, 501 (2002).

[59] N. Hanzawa, K. Saitoh, T. Sakamoto, T. Matsui, K. Tsujikawa, M. Koshiba, and F. Yamamoto, Mode multi/demultiplexing with parallel waveguide for mode division multiplexed transmission, Opt. Express **22**, 29321 (2014).

[60] S. H. Chang, H. S. Chung, R. Ryf, N. K. Fontaine, C. Han, K. J. Park, K. Kim, J. C. Lee, J. H. Lee, B. Y. Kim, and Y. K. Kim, Mode- and wavelength-division multiplexed transmission using all-fiber mode multiplexer based on mode selective couplers, Opt. Express **23**, 7164 (2015).

[61] S. G. Leon-Saval, T. A. Birks, J. B.-Hawthorn, and M. Englund, Multimode fiber devices with single-mode performance, Opt. Lett. **30**, 2545 (2005).

[62] Y. Sasaki, K. Takenaga, S. Matsuo, K. Aikawa, and K. Saitoh, Few-mode multicore fibers for long-haul transmission line, Optical Fiber Techn. **35**, 19 (2017).

[63] T. Sakamoto, T. Mori, M. Wada, T. Yamamoto, and F. Yamamoto, Coupled multicore fiber design with low intercore differential mode delay for high-density space division multiplexing, J. Lightwave Techn. **33**, 1175 (2015).

[64] C. Xia, N. Bai, I. Ozdur, X. Zhou, and G. Li, Supermodes for optical transmissions, Opt. Express **19**, 16653 (2011).

[65] N. K. Fontaine, R. Ryf, J. B.-Hawthorn, and S. G. L.-Saval, Geometric requirements for photonic lanterns in space division multiplexing, Opt. Express **20**, 27123 (2012).

[66] S. G. L.-Saval, N. K. Fontaine, J. R. S.-Gil, B. Ercan, R. Ryf, and J. B.-Hawthorn, Mode-selective photonic lanterns for space-division multiplexing, Opt. Express **22**, 1 (2014).

[67] Z. S. Eznaveh, J. E. Antonio-Lopez, J. C. A. Zacarias, A. Schülzgen, C. M. Okonkwo, and R. Amezcua Correa, All-fiber few-mode multicore photonic lantern mode multiplexer, Opt. Express **25**, 16701 (2017).

[68] T. A. Birks, I. Gris-Sánchez, S. Yerolatsitis, S. G. Leon-Saval, and R. R. Thomson, The photonic lantern, Advances in Optics and Photonics **7**, 107 (2015).

[69] B.-I. Popa and S. A. Cummer, Complex coordinates in transformation optics, Phys. Rev. A **84**, 063837 (2011).

[70] M. Moccia, G. Castaldi, V. Galdi, A. Alù, and N. Engheta, Dispersion engineering via nonlocal transformation optics, Optica **3**, 179 (2016).

[71] C. García-Meca and C. Barceló, Nontensorial transformation optics, Phys. Rev. Applied **5**, 064008 (2016).

[72] D. Marcuse, *Theory of Dielectric Optical Waveguides*, (Elsevier Academic Press, London, U.K., 1974).

[73] T. Mizuno, H. Takara, A. Sano, and Y. Miyamoto, Dense space-division multiplexed transmission systems using multi-core and multi-mode fiber, J. Lightwave Techn. **34**, 582 (2016).

[74] C. W. Hsu, B. Zhen, A. D. Stone, J. D. Joannopoulos, and M. Soljačić, Bound states in the continuum, Nat. Reviews **1**, 16048 (2016).

[75] M. S. Berger and N. S. Ussembayev, Isospectral potentials from modified factorization, Phys. Rev. A **82**, 022121 (2010).

[76] D. Dutta and P. Roy, Generalized factorization and isospectral potentials, Phys. Rev. A **83**, 054102 (2011).

[77] C. García-Meca, S. Carloni, C. Barcelo, G. Jannes, J. Sanchez-Dehesa, and A. Martínez, Transformational acoustic metamaterials based on pressure gradients, Phys. Rev. B **90**, 024310 (2014).

[78] S. Schmid, A. Härter, and J. H. Denschlag, Dynamics of a cold trapped ion in a Bose-Einstein Condensate, Phys. Rev. Lett. **105**, 133202 (2010).